

On the nature of the hard X-ray sources SWIFT J1907.3-2050, IGR J12123-5802 and IGR J19552+0044

F. Bernardini,^{1,2*} D. de Martino², K. Mukai^{3,4}, M. Falanga⁵, I. Andruchow⁶, J.-M. Bonnet-Bidaud⁷, N. Masetti⁸, D.H. Gonzalez Buitrago⁹, M. Mouchet^{10,11}, G. Tovmassian⁹

¹ Wayne State University, 666 W. Hancock Street, Detroit, MI, USA

² INAF – Osservatorio Astronomico di Capodimonte, Salita Moiarriello 16, I-80131 Napoli, Italy

³ CRESST and X-Ray Astrophysics Laboratory, NASA Goddard Space Flight Center, Greenbelt, MD 20771, USA

⁴ Department of Physics, University of Maryland, Baltimore County, 1000 Hilltop Circle, Baltimore, MD 21250, USA

⁵ International Space Science Institute (ISSI), Hallerstrasse 6, CH-3012 Bern, Switzerland

⁶ Facultad de Ciencias Astronomicas y Geofisicas, UNLP, and Instituto de Astrofisica La Plata, CONICET/UNLP, Argentina

⁷ CEA Saclay, DSM/Ifu/Service d'Astrophysique, F-91191, Gif-sur-Yvette, France

⁸ INAF – Istituto Astrofisica Spaziale, Via Gobetti 101, I-40129, Bologna, Italy

⁹ Instituto de Astronomia, Universidad Nacional Autonoma de Mexico, Apdo. Postal 877, Ensenada, Baja California 22800, Mexico

¹⁰ Laboratoire APC, Université Denis Diderot, 10 rue Alice Domon et Léonie Duquet, F-75005 Paris, France

¹¹ LUTH, Observatoire de Paris, Section de Meudon, 5 place Jules Janssen, F-92195 Meudon, France

Accepted 2013 July 30. Received 2013 July 25; in original form 2013 June 19

ABSTRACT

The *INTEGRAL* and *Swift* hard X-ray surveys have identified a large number of new sources, among which many are proposed as Cataclysmic Variables (CVs). Here we present the first detailed study of three X-ray selected CVs, Swift J1907.3-2050, IGR J12123-5802, and IGR J19552+0044 based on *XMM-Newton*, *Suzaku*, *Swift* observations and ground based optical and archival nIR/IR data. Swift J1907.3-2050 is highly variable from hours to months-years at all wavelengths. No coherent X-ray pulses are detected but rather transient features. The X-ray spectrum reveals a multi-temperature optically thin plasma absorbed by complex neutral material and a soft black body component arising from a small area. These characteristics are remarkably similar to those observed in magnetic CVs. A supra-solar abundance of nitrogen could arise from nuclear processed material from the donor star. Swift J1907.3-2050 could be a peculiar magnetic CV with the second longest (20.82 h) binary period. IGR J12123-5802 is variable in the X-rays on a timescale of $\gtrsim 7.6$ h. No coherent pulsations are detected, but its spectral characteristics suggest that it could be a magnetic CV of the Intermediate Polar (IP) type. IGR J19552+0044 shows two X-ray periods, ~ 1.38 h and ~ 1.69 h and a X-ray spectrum characterized by a multi-temperature plasma with little absorption. We derive a low accretion rate, consistent with a CV below the orbital period gap. Its peculiar nIR/IR spectrum suggests a contribution from cyclotron emission. It could either be a pre-polar or an IP with the lowest degree of asynchronism.

Key words: Cataclysmic Variables: general – stars: white dwarf – X-rays: individual: Swift J1907.3-2050 (also known as: V1082 Sgr), Swift J1212.3-5806 (also known as: IGR J12123-5802 and 1RXS J121222.7-580118), IGR J19552+0044, WISE J195512.47+004536.6

1 INTRODUCTION

Cataclysmic Variable stars (CVs) are binary system in which a white dwarf (WD) accretes matter from a late-type main sequence or subgiant star. A large fraction, $\sim 20 - 25\%$ (see e.g. Wickramasinghe & Ferrario 2000; Pretorius et al. 2013, and reference therein) of whole CV class, harbours magnetized WDs with

$B \gtrsim 10^5$ G up to 2.3×10^8 G. The high magnetic systems, the Polars, show intense and variable polarized emission in the optical and near-IR ranges, while those showing weakly or unpolarized optical/nIR emission, the Intermediate Polars (IPs), are believed to possess weaker $B \leq 10^6$ G. They are both characterized by variable X-ray emission at the rotational period of the accreting WD that is $P_{\text{rot}}/P_{\text{orb}} \simeq 1$ in the Polars (synchronous systems) and $P_{\text{rot}}/P_{\text{orb}} < 1$ in the IPs (asynchronous systems). The latter group is generally found above the 2–3 h orbital period gap, whilst the Po-

* E-mail: bernardini@wayne.edu

lars populate the orbital period distribution at short values, mainly below the gap (see Warner 1995).

The hard X-ray surveys carried out above 20 keV by the *INTEGRAL* and *Swift* satellites have detected more than a thousand of sources, a non-negligible fraction ($\sim 6\%$) of them are galactic X-ray binaries containing WDs (Barlow et al. 2006; Bird et al. 2010; Cusumano et al. 2010; Baumgartner et al. 2013). The confirmed CVs detected in these surveys are mainly magnetic of the IP type ($\sim 80\%$ of the whole sample). A few Polars and a handful of non-magnetic systems that include Dwarf Novae, old Novae and nova-like CVs, the latter still disputed to be magnetic, are also present. Finally, a few symbiotic stars have been also detected (see e.g. Luna et al. 2012). The current roster of these hard X-ray accreting WDs totals to 67, about half of them have been first proposed as CV candidates through optical spectroscopic follow-ups (e.g. Masetti et al. 2006, 2008, 2010, 2012) and many are suspected to harbour a magnetic WD. However, only X-ray follow-ups, mainly conducted with *XMM-Newton*, allowed to unambiguously confirm (de Martino et al. 2008; Anzolin et al. 2009; Scaringi et al. 2011; Bernardini et al. 2012; Masetti et al. 2012) or reject (de Martino et al. 2010, 2013) a CV identification, thanks to the detection (or non detection) of an X-ray signal at the WD spin period and to the characterization of the X-ray spectral properties. However, so far, there are several tens of sources to be still identified.

The role of CVs in the galactic population of X-ray sources has been quite discussed recently. In particular, magnetic CVs, are claimed to represent a large population (thousands of sources), and to be dominant contributors to the Galactic Ridge X-ray Emission (GRXE) and bulge emission (Revnivtsev et al. 2011; Hong et al. 2012; Hong 2012) at low luminosities (i.e. below 10^{33} erg s $^{-1}$). However, the bulk of the CV population that is dominated by non-magnetic short orbital period systems, can account for the very low end ($< 10^{30}$ erg s $^{-1}$) of the GRXE luminosity function (Reis et al. 2013), while magnetic CVs are believed to contribute most at $\gtrsim 10^{30}$ erg s $^{-1}$ (Hong 2012). The contribution from X-ray active stars at very low luminosities is still debated. The ratio of WD binaries and of coronally active stars is believed to be $\sim 2:1$ (Moriñana et al. 2013; Nebot Gómez-Morán et al. 2013).

In magnetic CVs, the accretion flow is magnetically channeled onto the WD polar regions. A strong shock is formed, below which matter cools via thermal bremsstrahlung and cyclotron radiation, the relative proportion primarily depending on the WD magnetic field strength (Woelk & Beuermann 1996; Fischer & Beuermann 2001). Hence, low-field magnetic CVs, like the IPs, have bremsstrahlung dominated shocks, while the Polars mainly cool via cyclotron radiation. Thus, IPs were initially known to be brighter X-ray sources than the Polars. However, before the deep surveys by *INTEGRAL* and *Swift* they only constituted a minor fraction of the magnetic CV subclass. This view has now changed with the identification of new magnetic systems of this type, suggesting that our knowledge of the magnetic CV population, and hence evolution, is still poor.

The identification of new hard X-ray CVs, can allow to put constraints on the true contribution of these binaries to the whole CV population as well as to identify new unexplored properties.

Most of the *INTEGRAL* and *Swift* hard X-ray CVs are found at long orbital periods ($\gtrsim 5$ h), with a few exceptions, and possess rapidly rotating WDs with spin-to-orbit period ratios ≤ 0.12 (Bernardini et al. 2012). This view could be confirmed or changed by the characterization of a larger sample, so that the role of system parameters, such as the WD magnetic field, the WD mass

and the mass accretion rate, can be finally unveiled. In this work, we present the first X-ray observations of a sample of three magnetic CV candidates, all hard X-ray sources: Swift J1907.3-2050, IGR J12123-5802 and IGR J19552+0044 (henceforth Swift J1907, IGR J1212, and IGR J1955). We complement the X-ray study with simultaneous UV and optical photometry acquired with the *XMM-Newton* satellite and with ground based optical and archival nIR/IR data. Swift J1907 is also known as V1082 Sgr, a long (20.82 h) orbital period CV suggested as a possible magnetic system by Thorstensen et al. (2010) because of the hard X-ray detection. IGR J1212 and IGR J1955 were identified by Masetti et al. (2010) from optical spectroscopic follow-ups as CVs and also suspected to be magnetic because of characteristics of their emission lines. No further information on these sources are available to date. Our study reveals unusual temporal and spectral properties that make these sources interesting cases for further follow-ups at other wavelengths.

2 OBSERVATIONS AND DATA ANALYSIS

2.1 *XMM-Newton* observations

The three sources were all observed in 2012 by the *XMM-Newton* observatory, (Turner et al. 2001; Mason et al. 2001; den Herder et al. 2001), using the EPIC Cameras as main instruments. The details of the *XMM-Newton* observations, together with that of *Swift* and *Suzaku* are reported in Tab. 1. All data were processed and scientific products were extracted with SAS version 12.0.1 using the latest calibration files (CCF) available in September 2012 (EPIC and OM) and May 2013 (RGS).

2.1.1 *The EPIC and RGS data*

All observations were performed with the EPIC PN and MOS cameras set in prime full window imaging mode with the thin filter. Standard data screening criteria were applied for all instruments.

For EPIC data, we extracted source photons from circular regions of radius $35''$ centred on source position determined by Gaussian fitting on one–dimension photon distribution. The background photons were extracted from a circular regions of same size within the same CCD.

To avoid contamination from solar flares in the spectral analysis we conservatively produced spectra using only those parts of the observations free from high background epochs. For the timing analysis we instead used the whole data sets except Swift J1907 for which contamination from solar flares is particularly strong at the end of the EPIC exposure. Background subtracted light curves were produced in the ranges: 0.3–15 keV (with a bin time of 15 s), 0.3–1 keV, 1–3 keV, 3–5 keV and 5–15 keV (with a bin time of 75 s). For each source, event arrival times were corrected to solar system barycenter. The EPIC spectra were rebinned before fitting, to have at least 30 counts per bin. We report the spectral analysis results obtained with the PN data only (consistency with the results of MOS cameras was always verified). Phase–resolved spectra were also extracted at the pulse maximum and minimum.

The RGS spectra were extracted using the whole exposures except Swift J1907 for which only the first 21 ks of data was retained. Due to low count rates, we only inspected the 1st order spectra for all 3 sources, however, for IGR J1212, even the 1st order spectra were too noisy to allow a spectral study. For Swift J1907 and IGR J1955,

we grouped channels so each had at least 16 source COUNTS, after ignoring extreme ends of the RGS energy ranges and the ranges corresponding to the inoperative CCD chips. Given the low statistical quality and the limited energy range of the RGS data, we used them mainly to confirm and refine the best-fit model derived using the EPIC data.

All spectra were analysed using the version of *XSPEC* (12.7.1n).

2.1.2 The Optical Monitor photometry

The Optical Monitor (OM) instrument was operated in fast window mode during all observations of the three sources. The OM data of Swift J1907 and of IGR J1955 were collected in two photometric bands using first the B filter, centered at 4500 Å and then the UVM2 filter, centered at 2310 Å. For IGR J1212 we instead used the V filter, centered at 5430 Å, due to brightness limits of a close-by star in the OM field of view. In this way we obtained two time series sets for each source 18.8 ks (Swift J1907), 16.6 ks (IGR J1212) and 15.8 ks (IGR J1955) long. The OM light curves were obtained from the SAS processing pipeline with a binning time of 10 s or 20 s. Corrections to the solar barycenter were also applied to the OM light curves.

2.2 The Suzaku observation

Swift J1907 was also observed with *Suzaku* (Mitsuda et al. 2007) in 2012 March, a few days after the *XMM-Newton* observation. Here we include the timing analysis of the data taken with the X-ray imaging spectrometer (XIS; Koyama et al. 2007). We have taken the data as processed using pipeline version 2.7.16.32, and extracted the source light curves from a circular region of 3.50' radius centered on the source image. Background light curves were extracted from an annular region with outer and inner radii of 6.25' and 4.50', respectively, and subtracted from the source region curves after scaling by the ratio of the extraction regions (0.65). Light curves from all 3 active XIS units have been combined in our analysis.

2.3 The Swift observations

The Swift Burst Alert Telescope, BAT (Barthelmy 2000), is a wide-field (~ 1 steradian) coded aperture mask instrument sensitive in the 14–195 keV range. Thanks to the large field of view, BAT has built up a sensitive all-sky map of the hard X-ray sky. We have taken the 8-channel spectra from the first 58-month of the mission¹. We collected BAT data of Swift J1907 and IGR J1212, while no data of IGR J1955 are available. IGR J1955 is also too faint to use the *INTEGRAL* IBIS/ISGRI spectral data, the source being at an average rate of 0.06 ± 0.02 c/s in the 20–40 keV². Therefore, we have extended the spectral analysis above 10 keV for Swift J1907 and IGR J1212 only.

The *Swift* X-ray Telescope (XRT, Gehrels et al. 2004) is an imaging CCD spectrometer sensitive in the 0.3–10 keV range. *Swift* performed 13 short (few ks) pointings of Swift J1907, 11 in 2008 and 2 in 2012. A total of about 35 ks of exposure time was collected on this source. We used the *Swift*/XRT data products generator at the University of Leicester (Evans et al. 2009) to build the background

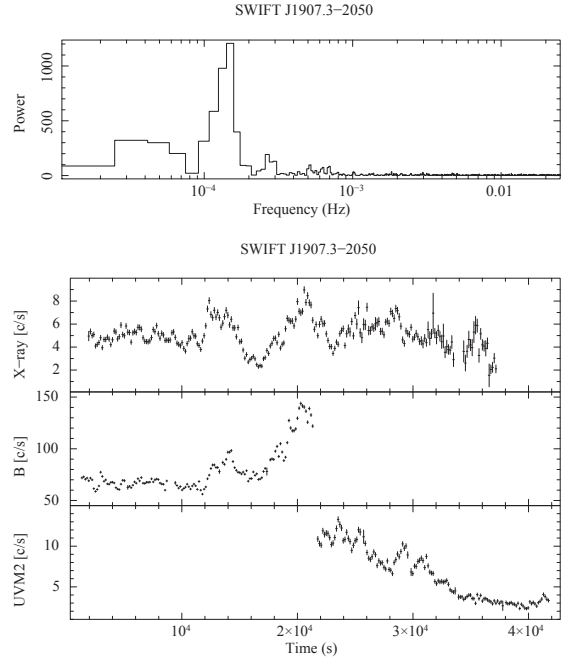


Figure 1. Upper Panel: Swift J1907 PN 0.3–15 keV power spectrum. Lower Panels: Swift J1907 background subtracted light curve in 3 energy bands: PN 0.3–15 keV (top), B (center), UVM2 (bottom). The binning time is 150 s in all bands.

subtracted light curve and the average spectrum in photon counting (PC) mode of Swift J1907.

3 RESULTS

3.1 Swift J1907.3-2050

3.1.1 X-ray Timing Analysis

The PN 0.3–15 keV light curve is highly variable (Fig. 1) with count rate changing by more than 60%. A long-term trend could also be present, with a timescale larger than 8 h, but the exposure (only 10.6 h) is not long enough to characterize this variability. The stronger variations are detected on shorter timescale (~ 2 h) after the first 10 ks since the start of the observation. The 0.3–15 keV power spectrum of the total observation (Fig. 1) shows an asymmetric peak at ~ 0.000139 Hz with an excess at lower frequencies. The first harmonic is also present and there is also indication of power at a lower frequency ($\sim 4 \times 10^{-5}$ Hz). The main peak would correspond to a period of 7200 ± 500 s (2.00 ± 0.14 h). All uncertainties are hereafter at 1σ confidence level if not otherwise specified. However, a closer inspection of the light curve in three time intervals: 0–10 ks, 10–25 ks, and 25–38 ks does not reveal pulses above 3σ significance, except in the 10–25 ks interval, where fractional variability is $32.7 \pm 0.6\%$. Therefore, the ~ 2 h X-ray signal does not appear to be coherent. The extracted light curves in the four energy bands 0.3–1, 1–3, 3–5 and 5–15 keV in the 10–25 ks time interval reveal that this transient variability is energy dependent, with fractional amplitude decreasing from $38 \pm 1\%$ in the 0.3–1 keV band to $28 \pm 1\%$ in the hard 5–15 keV band.

The *Suzaku* X-ray light curve, spanning over ~ 28.6 ks, includes a prominent brightening (hereafter “flare”) starting roughly halfway through the observation and lasting for 3 spacecraft orbits (5–6

¹ <http://swift.gsfc.nasa.gov/docs/swift/results/bs58mon/>

² <http://www.isdc.unige.ch/heavens/>

Table 1. Summary of main observations parameters for all instruments.

Source	Telescope	OBSID	Instrument	Date yyyy-mm-dd	UT _{start} hh:mm	T _{expo} (ks)*	Net Count Rate c/s		
Swift J1907.3-2050	<i>XMM-Newton</i>	0671850301	EPIC-pn	2012-03-19	11:32	38.0/13.6**	4.54 ± 0.02		
			EPIC-MOS1	2012-03-19	11:10	27.2	1.10 ± 0.07		
			EPIC-MOS2	2012-03-19	11:10	27.2	1.16 ± 0.07		
			RGS1	2012-03-19	11:10	36.5/20.9***	0.082 ± 0.003		
			RGS2	2012-03-19	11:10	36.5/20.9***	0.093 ± 0.003		
			OM-B	2012-03-19	11:20	18.8	79.82 ± 0.02		
			OM-UVM2	2012-03-19	17:00	18.8	6.52 ± 0.04		
			<i>Suzaku</i>	406042010	XIS0	2012-03-23	05:32	39.5	0.692 ± 0.004
			<i>Suzaku</i>		XIS1	2012-03-23	05:32	39.5	0.796 ± 0.005
			<i>Suzaku</i>		XIS3	2012-03-23	05:32	39.5	0.750 ± 0.005
	<i>Swift</i>	****	BAT			5800	3.5 ± 0.4 × 10 ⁻⁴		
			00037329001	XRT	2008-04-10	13:38	3.5	0.25 ± 0.01	
			00037329002	XRT	2008-06-04	15:57	0.4	0.13 ± 0.02	
			00037329003	XRT	2008-06-12	13:23	1.0	0.23 ± 0.02	
			00037329004	XRT	2008-06-12	15:01	0.3	0.23 ± 0.02	
			00037329005	XRT	2008-06-13	08:23	0.4	0.36 ± 0.03	
			00037329006	XRT	2008-06-13	10:20	0.1	0.36 ± 0.01	
			00037329008	XRT	2008-06-26	00:31	1.4	0.10 ± 0.01	
			00031252001	XRT	2008-08-19	06:54	1.3	0.05 ± 0.01	
			00031252002	XRT	2008-08-20	11:41	10.1	0.030 ± 0.003	
		00031252003	XRT	2008-08-28	07:36	1.9	0.05 ± 0.01		
		00037329009	XRT	2008-11-14	12:01	5.2	0.017 ± 0.002		
		00031252004	XRT	2012-06-19	12:32	3.4	0.002 ± 0.001		
		00031252005	XRT	2012-06-20	01:33	6.4	0.002 ± 0.001		
IGRJ12123-5802	<i>XMM-Newton</i>	0671850601	EPIC-pn	2012-01-07	15:48	37.4/12**	0.754 ± 0.008		
			EPIC-MOS1	2012-01-07	15:26	39.6	0.255 ± 0.003		
			EPIC-MOS2	2012-01-07	15:26	39.6	0.259 ± 0.003		
			RGS1	2012-01-07	15:25	40.1	0.010 ± 0.002		
			RGS2	2012-01-07	15:25	40.1	0.012 ± 0.002		
			OM - V	2012-01-07	15:35	15.8	2.33±0.03		
			OM - UVM2	2012-01-07	21:38	15.8	0.27±0.2		
			<i>Swift</i>	****	BAT			7500	1.8 ± 0.3 × 10 ⁻⁴
	IGRJ19552+0044	<i>XMM-Newton</i>	0671850201	EPIC-pn	2012-04-29	06:04	38/19**	2.88 ± 0.02	
EPIC-MOS1				2012-04-29	05:41	39	0.647 ± 0.005		
EPIC-MOS2				2012-04-29	05:41	39	0.630 ± 0.005		
RGS1				2012-04-29	05:41	36.8	0.054 ± 0.002		
RGS2				2012-04-29	05:41	36.8	0.071 ± 0.002		
OM-B				2012-04-29	05:50	15.8	4.87±0.02		
OM-UVM2				2012-04-29	10:40	15.8	0.65±0.02		

* Net exposure times.

** We report both the total exposure time and that after removing solar flares.

*** We report both the total exposure and that during the low background interval.

**** All available pointings are summed together.

hours). We have extracted the hard (>2 keV) and soft (<2 keV) light curves separately, but the hardness ratio does not show a significant change during the flare (Fig. 2). A Fourier analysis of the entire dataset (without energy cut) shows substantial power at low frequencies, including a peak near 2 hours, but no significant peaks at higher frequencies (Fig. 3). We analysed the flare and non-flare data separately and found that the 2 hour peak is not persistent through the observation; it is definitely absent in the non-flare data. While some power near this frequency may well be present in the flare data, no definite conclusion can be made due to the relatively short duration of the flare and the *Suzaku* orbital gaps.

We also inspected the *Swift*/XRT PC data of Swift J1907 to search

for similar variabilities. The source count rate changes along the total baseline (1533 d) from a maximum of ~ 0.5 c/s to a minimum of 0.002 c/s (see Fig. 4). In particular, we note that the two 2012 *Swift*/XRT observations carried out in June, three months after the *XMM-Newton* and *Suzaku* pointings, show the lowest count rate (0.002 c/s). Furthermore, hints for short term periodic-like variability, on the order of two hours, consistent with that measured in the *XMM-Newton* data, is found in a selected light-curve sub interval, where the *Swift* coverage was more dense (between $d \sim 132$ and $d \sim 132.4$ reference time BJD=2454567.0708). However, due to the satellite gaps we cannot further constrain this variability.

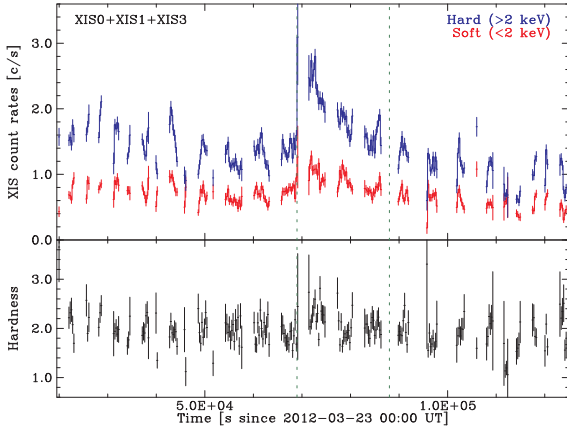


Figure 2. Swift J1907 : (Upper panel) *Suzaku*/XIS light curves of Swift J1907, in two energy bands. (Lower panel) The hardness ratio as a function of time. The vertical dashed lines define the flare interval used in Fourier analysis.

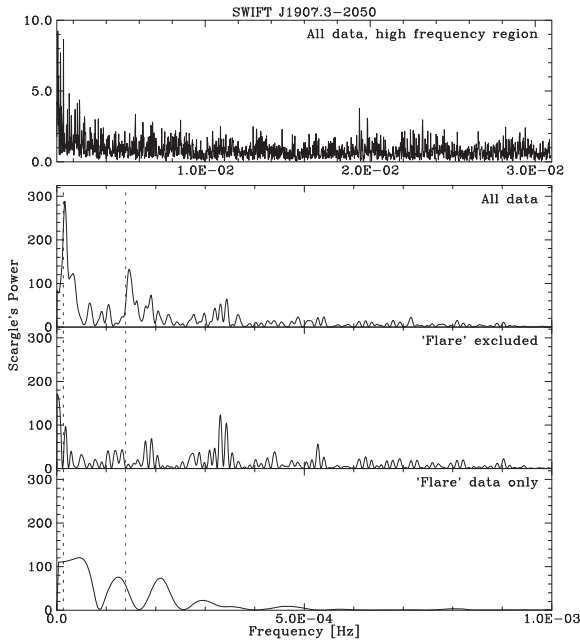


Figure 3. Swift J1907 : Power spectra of *Suzaku*/XIS data using Scargle's definition (Scargle 1982). The top panel shows the high frequency region of the power spectrum for all data. The bottom panels show the low frequency region, for the entire data, the non-flare data, and the flare data only, from top to bottom. The vertical dashed lines correspond to the 2 h variability detected in the *XMM-Newton* data.

3.1.2 The UV and optical light curves

Swift J1907 is at 13.14 ± 0.09 mag and at 14.70 ± 0.04 mag in the UVM2 and the B band, respectively, corresponding to fluxes of $1.43 \times 10^{-14} \text{ erg cm}^{-2} \text{ s}^{-1} \text{ \AA}^{-1}$ and to $1.03 \times 10^{-14} \text{ erg cm}^{-2} \text{ s}^{-1} \text{ \AA}^{-1}$.

The UV and optical light curves are also highly variable (see Fig 1) with a strong rise in the B band count rate after 12 ks, coincident in time with the X-ray flux increase. Both the X-ray and B light curves display a first maximum at ~ 13 ks and a second at ~ 20 ks. In the subsequent UV exposure the count rate decreases by a factor of 2.2 at the end of the pointing.

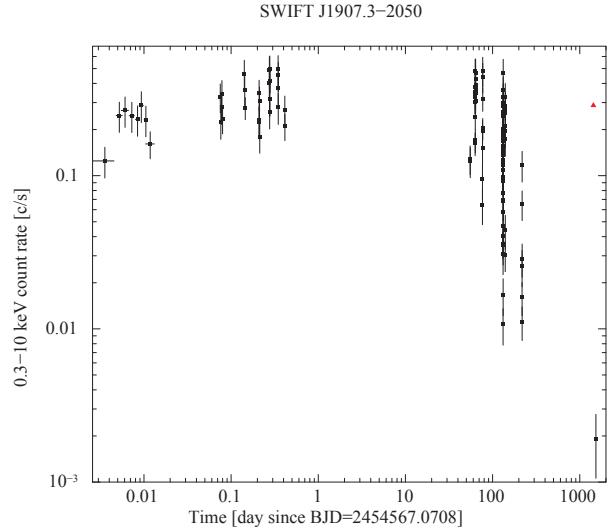


Figure 4. *Swift*/XRT light curve of Swift J1907. Due to the extremely sparse coverage, for plotting purposes, data are shown on a logarithmic scale. Black squares represent *Swift* data. The red triangle represent the estimated 0.5–10 keV *Swift* count rate for the *XMM-Newton* and the *Suzaku* 2012 pointings. We estimated it with *webpimms* using a power law multiplied by local and galactic absorption as a spectral model.

Table 2. Summary of the main timing results for the three sources. From left to right: $P_{1,2}^X$ (X-ray periods); P_{lt}^X (X-ray long term trend)

Source	$P_{1,2}^X$ ^a s	P_{lt}^X ^b h
Swift J1907	7200 ± 500 ^c	> 8.4
IGR J1212	-	7.6 ± 0.1
IGR J1955	$6100 \pm 120, 4960 \pm 80$	11.4 ± 0.2

^a 1σ cl.

^b 3σ cl. P_{lt}^X must be interpreted as an indication of long term variability.

^c This signal is not coherent.

We also divided the B band light curve in two intervals, I: 0–10 ks, and II: 10–22 ks, while we selected for the UVM2 light curve only the 22–38 ks interval (interval III). Then, we cross-correlated the X-ray (used as reference) with the B and UVM2 band light curves in the three intervals. The cross-correlation function (CCF) in interval II is broad and asymmetric towards negative lags, with degree of correlation 0.6. For CCFs with complex shapes or asymmetries the centroid is best evaluated using time lags in excess of 0.8 the peak value (e.g. Peterson et al. 1998; Shang 2002). We then find $t_{\text{cent}} \simeq -310$ s. The significance of the correlation is 15σ . Instead, no correlation is found in interval I, while for interval II a weak degree of correlation is found (0.2). Hence, we can then conclude that the optical light leads the X-rays in the II interval only and that the transient signal is also present at optical wavelengths.

3.1.3 X-ray Spectral analysis

The combined *XMM-Newton* EPIC and *Swift* BAT (0.3–100 keV) average spectrum was first fitted by a single optically thin component (MEKAL) multiplied by a complex absorption that includes a total absorber (WABS) and a partial covering absorber (PCFABS). The latter is justified by the energy dependence of the transient sig-

nal. This gives a poor fit ($\chi^2_\nu=2.05$ for 1000 dof). Substantial improvements are found including additional components and verifying their statistical significance (greater than 3σ) with an F-Test. We then obtain the best fitting model (see Fig. 5) consisting of two MEKAL components, a cold (c) at 0.12 ± 0.02 keV and a hot (h) at 13.2 ± 0.6 keV, plus an optically thick (BB) component at 61 ± 5 eV and a Gaussian, multiplied by a total and partial covering absorbers ($\chi^2_\nu = 1.15$ for 995 dof). No further component is required by the fit. The spectral parameters are reported in Tab. 3. The black body component, significant at 8σ confidence level, has a radius of 40^{+20}_{-10} km (at 1 kpc)³. The Gaussian accounts for the prominent emission feature at 6.4 keV with no significant energy shift. The total absorber column density is consistent with the galactic value in the direction of the source derived from Kalberla et al. (2005) and Dickey & Lockman (1990). No significant change with time is found in the spectral parameters within their statistical uncertainties.

The spectral analysis reveals that the X-ray emitting region is small and the plasma reaches typical temperatures achieved in a magnetically confined accretion flow, where a standing shock is formed at the poles of the compact star. Since the derived temperature of the hot component has to be regarded as a lower limit to the maximum temperature of the post-shock region (PSR), we also used the model of Suleimanov et al. (2005) (private code to be used into *Xspec*). This model takes into account the growth of pressure toward the WD surface and hence the change of gravity, allowing us to obtain a more reliable value for the maximum temperature and consequently an estimate of the WD mass. Since the model is computed for the continuum only, we then added a broad Gaussian to take into account the iron complex (thermal and fluorescence). A fit to the *XMM-Newton* EPIC and *Swift* BAT spectrum for $E > 3$ keV gives a mass $M = 0.64^{+0.03}_{-0.04} M_\odot$ ($\chi^2_\nu = 1.48$, 636 dof).

We inspected spectral parameters variability by comparing the *XMM-Newton* EPIC and *Swift*XRT spectra. Due to the low source count rate we accumulated an average XRT spectrum over all the *Swift* pointings in 2008, excluding the 2012 ones where the count rate is much lower. We used same model used for the EPIC spectrum, but did not include the 6.4 keV iron line and the BB component because they are not statistically required. We left free to vary all parameters except for the abundances that were fixed at the *XMM-Newton* best fit values. The spectral fit has a $\chi^2_\nu = 1.08$ for 114 dof. The temperature of the hot MEKAL is consistent, within uncertainties, with that found from the *XMM-Newton* spectral fit, ($kT_h = 14^{+4}_{-2}$ keV), while the temperature of the cold MEKAL is unconstrained, likely due to the low S/N. A 3σ upper limit is $kT_c < 0.11$ keV. The 0.3–10 keV *Swift* flux ($\sim 7.9 \pm 0.3 \times 10^{-12}$ erg cm⁻² s⁻¹) is a factor of ~ 3 fainter than that of *XMM-Newton* (see Tab. 3). We also extracted the June, 2012 XRT spectrum but used a simple power-law, due to the extremely low S/N. At this epoch the flux is: $6.1^{+7.9}_{-3.3} \times 10^{-14}$ erg cm⁻² s⁻¹, indicating a decrease by a factor of ~ 100 , in a three-months timescale. The *Suzaku* spectrum when fitted with the same components of *XMM-Newton* spectrum gives an average 0.3–10 keV flux of 2.3×10^{-11} erg cm⁻² s⁻¹, consistent with that obtained from the *XMM-Newton* data. From the long-term X-ray history (see also Fig. 4), we then conclude that Swift J1907 is also a highly variable X-ray source on months-years timescale.

³ A distance of $1.15^{+0.67}_{-0.42}$ kpc has been estimated by Thorstensen et al. (2010).

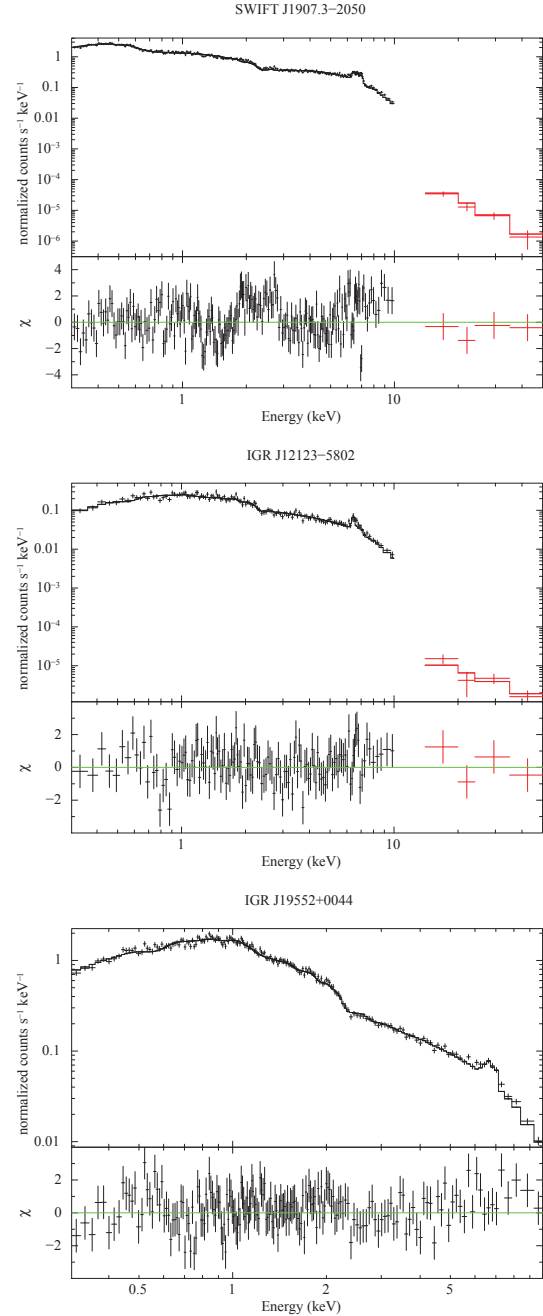


Figure 5. *Upper panels:* Swift J1907 broad band 0.3–100 keV count spectrum. Data are rebinned for plotting purposes. XMM data are in black while *Swift*/BAT data are in red. Residuals are shown in the bottom panel. *Center panels:* The same as above, but for IGR J1212. Here the CEMEKL model is shown. *Lower panels:* The same as above, but for IGR J1955, in the range 0.3–10 keV only (no BAT data are available). Here the CEMEKL model is shown.

3.1.4 The RGS spectrum of Swift J1907

We have applied the best fit EPIC model (Tab. 3) to the RGS spectra of Swift J1907 (Fig. 6). Although the overall trend is reproduced by the model, there are significant residuals and χ^2_ν remains relatively high (~ 1.3). The most prominent residuals correspond to the He-like lines of nitrogen ($E \sim 0.425$ keV). Using the variable abundance version of MEKAL model, fixing the abundances at 0.7 except

Table 3. Swift J1907: Spectral parameters of the best fitting model. Uncertainties are 1 sigma confidence level.

Swift J1907 BB+2 MEKAL		
N_{HW}	10^{22} cm^{-2}	0.103 ± 0.006
N_{HPc}	10^{22} cm^{-2}	9.6 ± 0.5
cvf	%	67 ± 1
kT_{BB}	eV	61 ± 5
kT_c	keV	0.12 ± 0.02
kT_h	keV	13.2 ± 0.6
R_{BB}	km	40_{-10}^{+20}
norm _c	10^{-3}	$5_{-0.9}^{+0.3}$
norm _h	10^{-3}	20.1 ± 0.5
A _Z		0.70 ± 0.05
EW*	keV	0.15 ± 0.01
F _{0.3-10}	10^{-11}	2.45 ± 0.05
F ₁₅₋₁₀₀	10^{-11}	1.3 ± 0.1
F ^{BB} **	10^{-11}	~ 2.9
F ^{bol} _{c+h} ***	10^{-11}	~ 12
χ^2_ν (dof)		1.15 (995)

* Gaussian energy fixed at 6.4 keV.

** Unabsorbed bolometric flux of the black body component.

*** Unabsorbed bolometric flux of the two optically thin components.

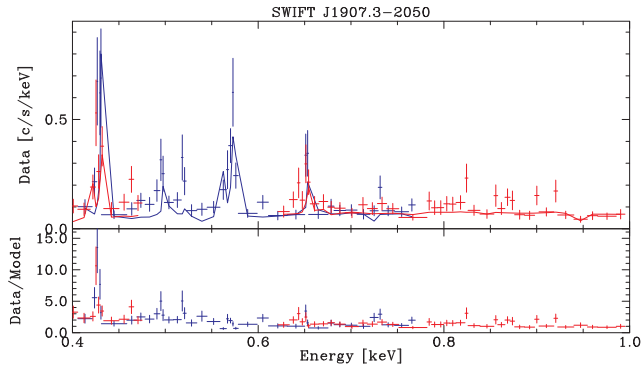


Figure 6. XMM-Newton/RGS spectra of Swift J1907 in the 0.4–1.0 keV region. RGS1 data are shown in blue, RGS2 in red. The top panel shows data with a model in which nitrogen abundance was left as free parameter, with a best-fit value of ~ 2 , while the abundances of other elements remain fixed at 0.7. The bottom panel shows the data to model ratio when the abundance of all elements were set to 0.7.

that of nitrogen, we find a significant overabundance of this element (~ 2 times Solar). While the χ^2_ν is still not satisfactory (~ 1.2), the modest quality of the RGS spectra and the large number of free parameters do not allow further possible refinement.

3.2 Swift J1212.3-5802

3.2.1 X-ray, UV and Optical timing analysis

The combined EPIC PN and MOS light curve in the 0.3–15 keV range (Fig. 7) shows the presence of a long term variability on which rapid changes by a factor of 2, occur on a timescale of tens of minutes. In the first 13 ks of observation the average count rate is $\sim 1.0 \text{ cts s}^{-1}$, between 13 ks and 30 ks the count rate is $\sim 0.6 \text{ c/s}$, while between 30 ks and 41 ks it is again $\sim 1.0 \text{ c/s}$. The power

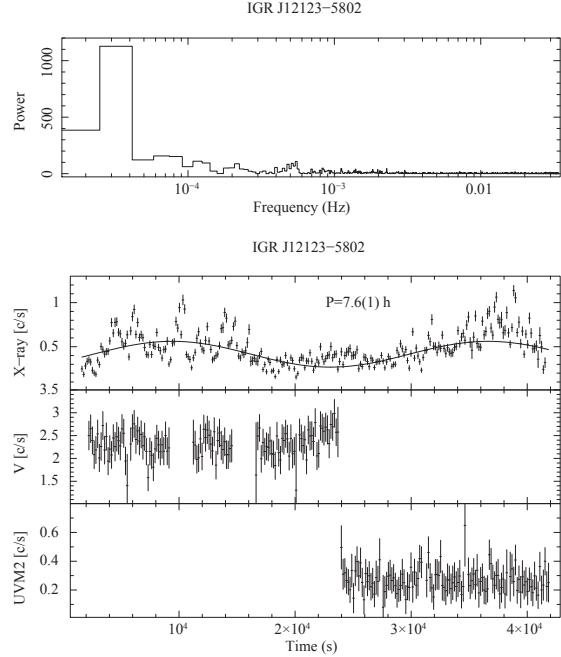


Figure 7. Upper Panels: IGR J1212 PN 0.3–15 keV power spectrum. Lower Panels: IGR J1212 PN plus MOS 0.3–15 keV background subtracted light curve (top), V band light curve (center), and UVM2 light curve (bottom). The binning time is 150 s in all bands. The solid line represents a fit made by a constant plus a sinusoid function (solid line).

spectrum shows a peak at $\sim 3.5 \times 10^{-5} \text{ Hz}$, $\sim 8 \text{ h}$ (see Fig. 7). A sinusoidal fit to the 0.3–15 keV light curve gives a period of $7.6 \pm 0.1 \text{ h}$, 3σ cl. Given that the XMM-Newton observation is 11.1 h long, we cannot assess if this variability is truly periodic.

The power spectrum of the light curve detrended from the main variability (7.6 h) does not reveal significant peak. A short term variability seems to be present during the high rate sections of the observation ($t \lesssim 18 \text{ ks}$, $t \gtrsim 30 \text{ ks}$) and the corresponding power spectrum peaks at 1900 s. However, this peak is only present in the first section. Hence, it is likely that at high rates IGR J1212 is affected by QPO-like variability. We also inspected the behaviour of HR with time, using both 1–3 keV/0.3–1 keV and 5–15 keV/3–5 keV ratios. No change is found within statistical uncertainties.

The OM V and UVM2 band photometry has low statistics, due to the faintness of the source ($V=17.1 \text{ mag}$ and $UVM2=17.2 \text{ mag}$), and does not show the changes observed in the X-rays (Fig. 7). We also analysed ground-based B band differential photometry acquired on 24–26 May 2011 at the 2.15 m telescope at the Complejo Astronomico el Leoncito, CASLEO, in Argentina, equipped with a direct CCD camera. IGR J1212 was observed for about 5 h each night. Exposure times of individual images were 60, 90 and 120 s respectively. The B band light curve (not shown) displays flickering-type variability on timescales from few minutes to tens of minutes with no clear periodic trend during the three nights.

3.2.2 X-ray Spectral analysis

We found two spectral models that are equally statistically acceptable. The first one is composed by a multi-temperature optically thin plasma in which the emission measure follows a power-law in temperature (CEMEKL) plus a Gaussian at 6.4 keV to account for the fluorescent 6.4 keV Fe line. The power-law index α , when left

free to vary is consistent within errors to unity. We, therefore, fixed it at this value. The second one is made by the sum of two MEKAL and a Gaussian at 6.4 keV. Both models required a complex absorption made of a total (WABS) and a partial covering (PCFABS) absorbers. In both cases, the inclusion of a black body component is not statistically required, its significance being $< 2\sigma$. Spectral fit results are reported in Tab. 4 and shown in Fig. 5 (CEMEKL model only).

The hydrogen column density of the total absorber is lower than the total galactic column density in the direction of the source ($3.2\text{--}4.1 \times 10^{22} \text{ cm}^{-2}$), suggesting an interstellar origin. On the other hand the N_{H} of the partial covering absorber ($\text{cvf} = 49\text{--}53\%$) indicates it is local. For both models, CEMEKL and two-MEKAL, the high temperature component is unconstrained. Lower limits of 43 keV and 62 keV are found, respectively. The 6.4 keV fluorescent Fe line is strong in this source ($\text{EW} = 250 \text{ eV}$) indicating that reflection is not negligible. However, a reflection component is not statistically significant in the fits. In both cases the abundances are, within uncertainties, consistent with the solar value. We are unable to prefer one of the two models with current data. To estimate the WD mass, we applied also for this source the Suleimanov et al. (2005) model obtaining $M_{\text{WD}} = 0.89^{+0.02}_{-0.04} M_{\odot}$. The 0.2–10 keV spectrum, extracted between 0–14 ks (high rate) and 14–30 ks (low rate), if fitted with the same model does not reveal spectral changes within statistical uncertainties, except for the normalization. Hence, the large variability observed during the *XMM-Newton* exposure is due to changes of the emitting volume.

3.3 IGR J19552+0044

3.3.1 X-ray timing analysis

IGR J1955 is also a highly variable source. The 0.3–15 keV combined EPIC PN and MOS light curve displays a large amplitude variation over the whole observation where count rate increases by a factor ~ 3 (Fig. 8). A dip lasting ~ 1.5 ks is also observed at ~ 10 ks since the start of the observation. The count rate decreases by ~ 9.7 times the average value, almost reaching zero counts. A short term (few hours) variability is also present.

The X-ray power spectrum shows three main peaks: a short frequency one at $\sim 2.5 \times 10^{-5} \text{ Hz}$ ($\sim 11 \text{ h}$), and two close ones at $\sim 1.7 \times 10^{-4} \text{ Hz}$ and $2 \times 10^{-4} \text{ Hz}$ ($\sim 6000 \text{ s}$ and $\sim 5000 \text{ s}$) respectively (see Fig. 8). A sinusoidal fit to the light curve gives a period of $11.4 \pm 0.2 \text{ h}$ ($3\sigma \text{ cl}$). This value should be considered as an indication of a long term variability, because of the limited *XMM-Newton* exposure. For the two short term variabilities, both significant at $8\sigma \text{ cl}$, we obtain: 6100 ± 120 ($1.69 \pm 0.04 \text{ h}$) and $4960 \pm 80 \text{ s}$ ($1.32 \pm 0.08 \text{ h}$). On the other hand the UV and B band light curves are too short to allow a timing study. However, we can identify an optical counterpart (B band), although much shallower, to the dip observed in the X-rays (see Fig. 8).

We studied the energy dependence of the pulse shape, by fitting the light curves in the ranges 0.3–1 keV, 1–3 keV, 3–5 keV and 5–15 keV at the two periods. The pulse at 4960 s is phase aligned and structured at all energies, with a double peaked maximum at phases ~ 0.0 and ~ 0.3 respectively. The pulse fraction PF^4 slightly decreases with energy: $\text{PF}_{0.3-1} = 18.2 \pm 0.8\%$, $\text{PF}_{1-3} = 16.5 \pm 0.8\%$, $\text{PF}_{3-5} = 20 \pm 2\%$, $\text{PF}_{5-15} = 13 \pm 2\%$. The

⁴ The pulse fraction is here defined as: $\text{PF} = (A_{\text{max}} - A_{\text{min}}) / (A_{\text{max}} + A_{\text{min}})$ where A_{max} and A_{min} are respectively the maximum and minimum value of a sinusoidal function.

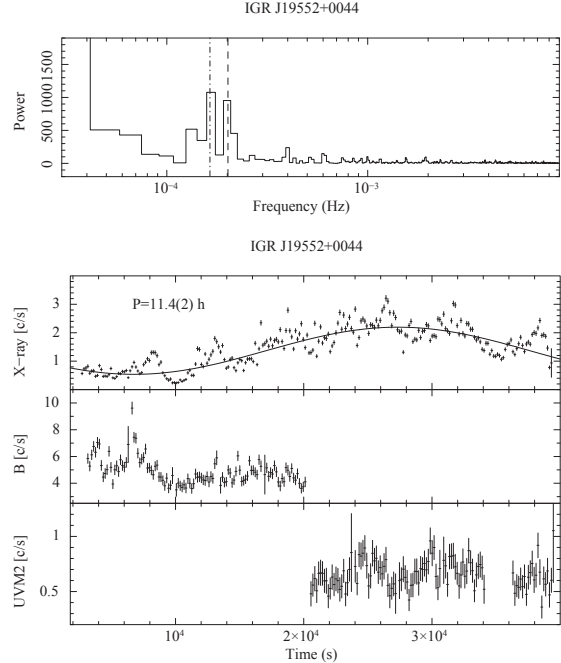


Figure 8. *Upper Panel:* IGR J1955 PN 0.3–15 keV power spectrum. The dashed and dot dashed lines at $\sim 1.7 \times 10^{-4} \text{ Hz}$ and 2×10^{-4} represent the 1.69 h and 1.32 h periods, respectively. *Lower Panels:* IGR J1955 PN plus MOS 0.3–15 keV background subtracted light curve (top), B band light curve (center), and UVM2 light curve (bottom). The binning time is 150 s in all bands. The solid line represents a fit made by a constant plus a sinusoid function (solid line).

average PF in the 0.3–15 keV range is $17.0 \pm 0.5\%$. The hardness ratio (HR) between 1–3 keV and 0.3–1 keV indicates a tendency of spectral hardening (significant at 3.6σ level) close to pulse minimum, $\phi = 0.4\text{--}0.6$ (see Fig. 9). The low S/N does not allow to infer changes in the HR between 5–15 keV and 3–5 keV bands.

The pulse at 6100 s is instead less structured and roughly single peaked, with the maximum at $\phi = 0.2$, phase aligned at all energies. The PF slightly increases with energy: $\text{PF}_{0.3-1} = 14.6 \pm 0.8\%$, $\text{PF}_{1-3} = 18.5 \pm 0.8\%$, $\text{PF}_{3-5} = 20 \pm 2\%$, $\text{PF}_{5-15} = 22 \pm 2\%$. The average PF in the total 0.3–15 keV band is $17.1 \pm 0.5\%$. A marginally significant (2.4σ) spectral hardening at pulse maximum is found from the HR between 1–3 keV and 0.3–1 keV bands.

Finally, the HR between 1–3 keV and 0.3–1 keV over the whole *XMM-Newton* observation reveals a hardening when flux increases. The ratio between the two light curves is 0.78 ± 0.03 during the first 6 ks, while later it is 1.18 ± 0.02 .

3.3.2 X-ray spectral analysis

The best fit model is made of a multi-temperature (CEMEKL) plasma absorbed by a total absorber (WABS) and a Gaussian to account for the excess at 6.4 keV. The inclusion of a partial covering absorber (PCFABS) is not statistically required. The power law α index is 0.74 ± 0.05 and its inclusion as free parameter is significant at 4.8σ . The N_{H} column density is $0.07 \pm 0.02 \times 10^{22} \text{ cm}^{-2}$, and is lower than the total galactic column density in the direction of the source ($0.13\text{--}0.16 \times 10^{22} \text{ cm}^{-2}$). The fluorescent 6.4 keV Fe line is moderately weak ($\text{EW} = 70 \pm 20 \text{ eV}$). A soft black body component is not required. All model parameters are reported

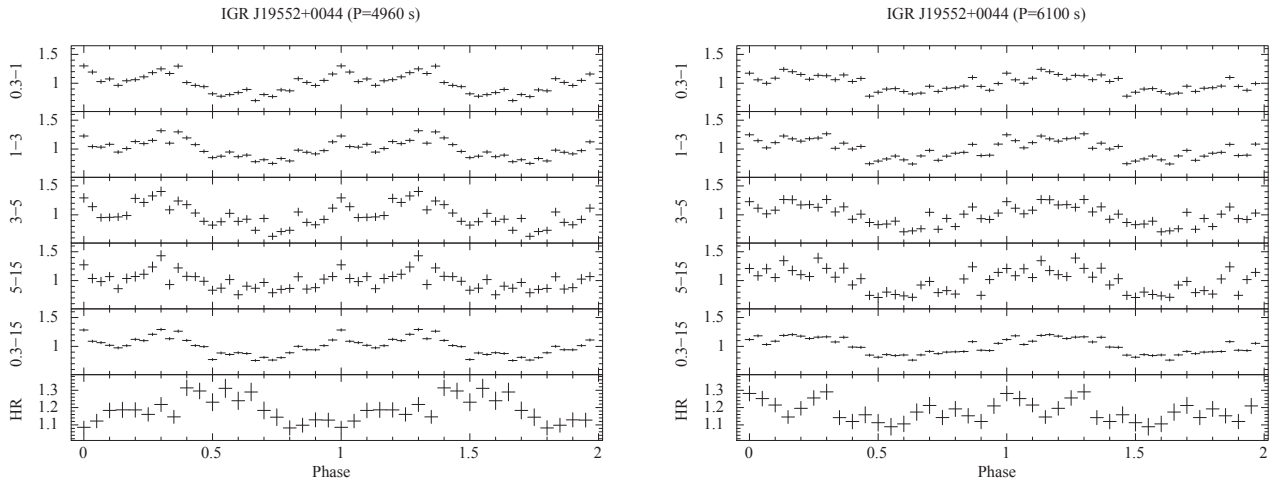
Table 4. IGR J1212: spectral parameters of the best fitting models. Uncertainties are 1 sigma confidence level.

IGR J1212					
CEMEKL			2 MEKAL		
N_{H_W}	10^{22} cm^{-2}	0.11 ± 0.01	N_{H_W}	10^{22} cm^{-2}	0.11 ± 0.01
$N_{H_{Pc}}$	10^{22} cm^{-2}	2.3 ± 0.4	$N_{H_{Pc}}$	10^{22} cm^{-2}	2.8 ± 0.5
cvf	%	53 ± 3	cvf	%	49 ± 2
kT_{max}	keV	>43	kT_c	keV	5.95 ± 0.02
norm	10^{-3}	6.4 ± 0.3	kT_h	keV	>62
A_Z		1.0 ± 0.3	norm _c	10^{-3}	0.5 ± 0.2
EW*	keV	0.25 ± 0.03	norm _h	10^{-3}	2.6 ± 0.5
$F_{0.3-10}$	10^{-11}	0.46 ± 0.01	A_Z		1.5 ± 0.4
F_{bol}^{**}	10^{-11}	1.5 ± 0.1	EW	keV	0.21 ± 0.03
χ^2_{ν} (dof)		0.93 (261)	$F_{0.3-10}$	10^{-11}	0.46 ± 0.02
			F_{15-100}	10^{-11}	0.77 ± 0.01
			$F_{bol}^{c+h}^{***}$	10^{-11}	1.6 ± 0.1
			χ^2_{ν} (dof)		0.87 (259)

* Energy of the Gaussian fixed at 6.4 keV.

** Unabsorbed bolometric flux of CEMEKL model.

*** Unabsorbed bolometric flux of the MEKAL components.


Figure 9. *Left panels:* From top to bottom, IGR J1955 pulse profiles folded at 4960 s in five energy intervals, 0.3–1, 1–3, 3–5, 5–15, 0.3–15 keV, on the y axis the normalized intensities. On the bottom line the Hardness Ratio (HR) for the 1–3 keV vs 0.3–1 keV band. *Right panels:* The same as left panels, but for the 6100 s period.

in Tab. 5 (see also Fig. 5). Similarly to the other sources, we also applied the Suleimanov et al. (2005) model to derive the WD mass, and find $M_{WD} = 0.77^{+0.02}_{-0.03} M_{\odot}$ ($\chi^2_{\nu} = 1.09, 489$ dof).

We also investigated phase-dependent spectral variability at the 4960 s period, by selecting the phase intervals $\phi = 0.0 - 0.5$ and $\phi = 0.5 - 0.9$ corresponding to the maximum and minimum respectively. We fixed at their average values the hydrogen column density N_H , the metal abundance A_Z , and the Gaussian energy, all other parameters were left free to vary. Only the normalization was found to change ($\sim 20\%$) according to the flux variation.

The RGS spectra have low S/N but broadly confirm the EPIC spectral fits. The strongest lines seen are those of OVII, OVIII, and FeXVII (0.83 keV=15Å). Some lines (N VII, O VII, Mg XI and Mg XII) may be stronger than that in the best fit model. However, this should be re-examined with higher S/N data.

4 DISCUSSION

4.1 Swift J1907.3-2050: a long period magnetic CV?

The X-ray history of Swift J1907 over ~ 5 yr reveals a highly variable X-ray source on both short (hours) and long (months-years) time scales. We detect a transient feature with characteristic timescale of ~ 2 h in the *XMM-Newton* X-ray and optical data. It may also be present in the *Suzaku* and *Swift* XRT data at some epochs. The possibility that it represents the spin period of the WD is highly unlikely, since the spin signal is not expected to disappear without a significant change in the source state. The characteristic 2 h timescale is close to the free-fall time from the inner Lagrangian point. Indeed, with a WD mass of $0.64 M_{\odot}$ and a donor star mass of $0.8 M_{\odot}$ (Thorstensen et al. 2010), this binary would have an inverted mass ratio $q = M_{\text{sec}}/M_{WD} = 1.3$. The WD Roche Lobe radius would be 1.8×10^{11} cm and the free-fall time ~ 5900 s. The occurrence of this feature at high rates (both in the X-rays

Table 5. IGR J1955: spectral parameters of the best fitting model. Uncertainties are 1 sigma confidence level

IGR J1955 CEMEKL		
N_H	10^{22}cm^{-2}	0.076 ± 0.003
kT_{max}	keV	36 ± 4
norm	10^{-3}	9.9 ± 0.4
α		0.74 ± 0.05
A_Z		0.62 ± 0.07
EW*	keV	0.07 ± 0.02
$F_{0.3-10}$	10^{-11}	1.06 ± 0.01
F_{bol} **	10^{-11}	2.2 ± 0.1
χ^2_{ν} (dof)		1.05 (725)

* Energy of the Gaussian fixed at 6.4 keV.

** Unabsorbed bolometric flux of CEMEKL model.

and UV/optical) suggests a transient enhancement of mass transfer from the donor star overflowing the accretion disc. For the latter we estimate a color temperature of 12 kK from the lowest observed UV and B band fluxes corrected for reddening⁵. The flare activity also indicates that mass accretion rate changes are not uncommon on timescales of hours.

Swift J1907 also varies on a longer time scale ($\gtrsim 8$ h) in both X-ray and optical/UV ranges and we could detect a flare-like activity lasting ~ 6 h in the *Suzaku* data. With the present data we cannot assess whether it is related to the long 20.82 h orbital period. Due to the lack of energy dependence the flare is likely due to a temporary enhancement in the accretion rate, rather than resulting from an orbital modulation.

Swift J1907 was already known to display high, intermediate and low optical states, where accretion partially or completely switches-off in some occasions (see Thorstensen et al. 2010, and reference therein). The X-ray history also shows that it undergoes high and low X-ray states on a months-years time scale, thus corroborating mass accretion rate changes. This peculiarity is typical of magnetic systems of the Polar type or nova-like CVs of the VY Scl type stars (see e.g. Honeycutt & Kafka 2004). The orbital period of 20.82 h is by far longer than those of VY Scl stars, which cluster at the 3 h edge of the orbital period gap, and also longer than those of Polars, being V1309 Ori (8 h) the longest period Polar known so far.

The spectral characteristics of Swift J1907 may favour a magnetic system as early suggested by Thorstensen et al. (2010). A high complex absorbing material, is a defining characteristic of magnetic systems, particularly of IPs, rather than of non-magnetic CVs (see Ramsay et al. 2008). Also a multi-temperature plasma reaching high temperatures (~ 14 keV) is typical of accretion shocks at the WD poles. An optically thick component, with temperature of 60 eV and with a small emitting area, is also a characteristic of magnetic systems only. This component is a recognized feature in Polars and recently in IPs. However, an orbitally-locked WD rotation at the extremely long 20.82 h period would imply a very high magnetic field, $\gtrsim 1.4 \times 10^{10}$ G (see Warner 1995). No WD in CVs has ever been detected with such magnetic field

⁵ We adopt an extinction of $E_{B-V} = 0.14$, as derived from the hydrogen column density from X-ray spectral fits (Ryter et al. 1975).

strength, being the highest field Polar AR UMa with $B = 2.3 \times 10^8$ G. At high field strengths accretion shocks are cyclotron dominated and even buried at low local accretion rates (Woelk & Beuermann 1996; Fischer & Beuermann 2001). This would yield a strong soft component. We instead infer a bolometric flux ratio between the black body and optically thin components $F_{\text{BB}}/F_{\text{thin}} \sim 0.24$.

The remaining possibility is that Swift J1907 is an IP. This would be consistent with the spectral characteristics of this sub-type of magnetic systems. Known IPs at the longest ($\gtrsim 10$ h) periods, such as GK Per (47.9 h), RX J1730-0559 (15.4 h) and AE Aqr (9.9 h), possess rapidly spinning WDs with high degree of asynchronism (≤ 0.002), with the only exception of V1062 Tau (10 h, and ~ 0.1). However, no rapid X-ray pulses are detected in the X-ray power spectrum of Swift J1907.

The presence of a black body component at 60 eV, with a ratio between the bolometric soft and hard X-ray fluxes of about 0.24, is a key signature of magnetic accretion. Typical range of temperatures in Polars is 20–40 eV, with a few systems at ~ 60 eV. In IPs the soft component is instead found to span a wider range of temperatures up to ~ 90 eV (Anzolin et al. 2008, 2009; Bernardini et al. 2012). Hence Swift J1907 is located in the soft-to-hard X-ray luminosity ratio vs temperature plane (see Anzolin et al. 2008) midway between the Polars and IPs. In Swift J1907 this component arises from a small region of 40 km (a 3σ upper limit is 114 km at 1 kpc). For a WD mass of $0.64 M_{\odot}$ the corresponding radius is 8.3×10^8 cm (Nauenberg 1972), implying that the reprocessed optically thick emission comes from a fractional area $f \sim 6 \times 10^{-6}$ (3σ upper limit is $f \lesssim 2 \times 10^{-4}$). It was recently demonstrated that this soft X-ray component is constituted by a range of temperatures over the accretion spot area (Beuermann et al. 2008, 2012). The projected fractional WD surface area in the prototypical Polar AM Her is about 0.07% with the hottest regions (> 40 eV) arising from much smaller fractional areas, $< 2 \times 10^{-6}$ (see Beuermann et al. 2012, for detail). For Swift J1907 we can only infer the average temperature of this component and a rather small and weakly constrained emitting area. These values are closer to those derived in the soft IPs (Anzolin et al. 2008), which seem to possess smaller and hotter spots than Polars. Hence, though sharing similar properties of soft emitting magnetic CVs, it cannot be unambiguously ascribed to either the IP or the Polar groups.

To help in understanding this CV, we also estimated its mass accretion rate. We assume that the accretion luminosity is represented by the X-ray bolometric luminosity, $L_{\text{acc}} = G \dot{M} M_{\text{WD}} R_{\text{WD}}^{-1} \sim L_{\text{BB}} + L_{\text{thin}}$, that includes both reprocessed X-ray component and that of the hard X-rays. Using the derived WD mass and radius values of $0.64 M_{\odot}$ and 8.3×10^8 cm, we estimate $\dot{M} = 2 - 4 \times 10^{-9} M_{\odot} \text{yr}^{-1}$, for a minimum distance of 730 pc and a maximum of 1.15 kpc respectively. This value is higher than the mass transfer rate ($\dot{M}_{\text{sec}} \sim 5 \times 10^{-10} M_{\odot} \text{yr}^{-1}$) expected for a donor filling its Roche lobe (Warner 1995) at a 18-20 h orbital period. It is however lower by two orders of magnitude than that predicted by magnetic braking (McDermott & Taam 1989) at the same orbital periods. Consequently, it may be possible that Swift J1907 has recently entered into a CV phase. The high nitrogen abundance is also a peculiar feature of Swift J1907. A number of CVs were found from far-UV spectra to display anomalous CNO abundance and believed to be descendant of massive progenitor donors (Gänsicke et al. 2003). This, together with the large binary mass ratio and the long orbital period, might suggest that Swift J1907 is also descending from a progenitor binary which underwent a phase of thermal time-scale mass transfer (TTMT Schenker et al. 2004; Podsiadlowski et al. 2003).

Further long observations in the X-rays and in the optical, including polarimetry as well as UV spectroscopy, will help to understand the true nature and evolutionary status of this CV.

4.2 IGR J12123-5802 a true IP or a magnetic impostor?

IGR J1212 is a faint, but highly variable X-ray source. We find a $\gtrsim 7.6$ h variability although we cannot assess whether it is related to the binary orbit. Variations on time scales of ~ 1900 s are not periodic. None of these variabilities have an optical counterpart where only flickering on timescale of a few minutes is found.

On the other hand, the broad-band X-ray spectrum is hard and well described by a multi-temperature plasma with a high, although unconstrained, maximum temperature. We also infer a high mass for the WD ($0.89M_{\odot}$). The spectrum is highly absorbed by interstellar and local material, the latter covering $\sim 50\%$ the X-ray source. A strong (EW = 250 eV) Fe fluorescent line is also present suggesting that reflection from cool material is present in this system. A high column density partial absorber and an intense Fe fluorescent line are defining characteristics of magnetic CVs (Ezuka & Ishida 1999). Hence, a magnetic system might be favoured. The lack of detection of a black body component also does not favour a Polarity CV. While the lack of detection of a coherent periodicity does not allow us to classify IGR J1212 as an IP, we here note that other systems, such as LS Peg, EI UMa and V426 Oph (Ramsay et al. 2008), have also failed to show coherent periodicities and due to the spectral characteristics similar to IPs, were defined as "bona fide" IPs. For V426 Oph and LS Peg it is also speculated that the lack of pulsations could be due to the close alignment of the magnetic and rotation axes.

The high temperature derived from X-rays if due to magnetic accretion would imply a mass of $0.89M_{\odot}$, that would locate IGR J1212 within the range of most CV primary masses (Zorotovic et al. 2011). On the other hand if this temperature is achieved through a Keplerian disc accretion it would give a WD mass of $\sim 1.2M_{\odot}$. Few CVs are known to harbour such massive WDs (Zorotovic et al. 2011).

Optical spectroscopy and polarimetry, as well as long photometric runs, could help to shed light into this new CV.

4.3 IGR J19552+0044: a long period IP or a magnetic CV below the gap?

We have detected periodic variabilities at 1.69 h (6100 s), 1.38 h (4960 s). A large amplitude variability on timescale of 11 h is also present. Support to both the short and the long term variabilities also comes from optical ground-based photometry and spectroscopy (Tovmasian et al. in preparation, private communication). The X-rays arise from a multi-temperature plasma with maximum temperature of 36 keV suffering little absorption of interstellar origin. The 1.38 h periodicity is due to changes in the normalization of the emitting plasma. These features are rather similar to HT Cam (de Martino et al. 2005), a low accretion rate IP below the orbital period gap. The bolometric X-ray luminosity is $4.3 \times 10^{31} d_{100\text{pc}}^2 \text{ erg s}^{-1}$. If it represents the accretion luminosity, for $M_{\text{WD}} = 0.8M_{\odot}$ and $R_{\text{WD}} = 7 \times 10^8 \text{ cm}$ (Nauenberg 1972), the accretion rate would indeed be very low: $4.5 \times 10^{-12} d_{100\text{pc}}^2 M_{\odot} \text{ yr}^{-1}$.

The X-ray periodicities of 1.69 h, 1.38 h and the ~ 11 h variability are, however, difficult to interpret. We here propose and discuss two possibilities.

4.3.1 A long period IP or a pre-Polar?

If 1.38 h represents the spin of the accreting WD and 1.69 h is a sideband period ($P_{\omega-\Omega}$ or $P_{\omega-2\Omega}$), the orbital period would be either 7.3 h or 14.6 h. The detected variability at 11 h or longer, if periodic, would suggest the second case. However, such long-period system is expected to have a high accretion rate and a main sequence G3-5 type donor star (Smith & Dhillon 1998). A re-analysis of the optical spectra by Masetti et al. (2010) does not reveal G-type star features but only weak absorptions in the red portion, possibly suggesting Ca I 6162 Å, and TiO 6900 Å. Hence a G-type star is rather unlikely. The 2MASS measures give only an upper limit to the J band magnitude ($J < 17.03$), implying a lower limit to the distance of 6.4 kpc which seems to be in contradiction with the inferred low absorption. Furthermore, the ratios of He II and H_{β} line fluxes and equivalent widths (EWs) are closer to those found in Polars rather than in IPs (van Paradijs & Verbunt 1984) and the overall spectrum very much resembles those of Polars. Also, IGR J1955 is found at $B=17.6$ mag, at similar flux level when observed by Masetti et al. (2010) in 2009, but much fainter than in the USNO (15.6 mag) and in the Sloan Digital Sky Survey (SDSS) catalogues ($g=15.9$ mag). A 1.6–2 mag difference suggests a highly variable source, that is more common to short period CVs.

Alternative possibility is that the 1.38 h and the 1.69 h periods are the spin and the orbital periods, respectively. A short period magnetic CV could reconcile the low accretion rate and the absence of intrinsic absorption derived from X-rays. The beat period would then be 7.29 h, not detected but the long term variability could be a sign of a sub-harmonic, although difficult to interpret. Clearly a longer observation would solve the true nature of the long-term variability. If it were the case the spin-to-orbital period ratio would be 0.82. The period of 1.69 h would locate this source below the orbital period gap, where most Polars are found and only five IPs. The latter have spin-to-orbit period ratio ranging from 0.1 (HT Cam) to 0.68 (EX Hya). On the other hand, only five Polars are known to possess desynchronized primaries (CD Ind, BY Cam, V1500 Cyg, V4633 Sgr and V1432 Aql) with spin-to-orbital period ratios between 0.98 and 1.02. IGR J1955 would then be either an extremely low asynchronous IP or the most asynchronous Polar. Only one system is known to share a similar property, Paloma also known as RX J0524+42 (Schwarz et al. 2007). Its spin-to-orbit period ratio of 0.93–0.97 (depending on the true spin period) and its orbital period of 2.6 h locate it in the period gap. Paloma is believed to be a transition object between IPs and Polars. As no IP is theoretically expected below the orbital period gap, the few IPs will likely never synchronize (Norton et al. 2004, 2008). However, IGR J1955 being so close to the line of synchronization could still evolve towards synchronism. In this case magnetic field measurements through polarimetry are crucial.

The X-ray analysis also reveals a hard X-ray spectrum but no soft X-ray black body component. Three of the asynchronous Polars mentioned above (CD Ind, BY Cam, and V1432 Aql) display unusually hard X-ray spectra and are detected above 20 keV in the INTEGRAL/IBIS or Swift/BAT surveys. Interestingly also Paloma has been detected by Swift/BAT and has been recently catalogued in the latest 70-month BAT catalogue (Baumgartner et al. 2013).

4.3.2 A magnetic evidence from IR

IGR J1955 is reported in the 2MASS catalogue with $J < 17.03$ mag, $H = 15.63 \pm 0.11$ mag, and $K = 14.07 \pm 0.06$ mag. The J band upper limit could be due to the drop of the UV-optical spectrum

at these wavelengths, but the 2MASS color index $(H-K)=1.56$ does not support the contribution from any donor late type star (see Straizys & Lazauskaitė 2009). If the 2MASS J band upper limit is attributed to a M5 star (for an orbital period of 1.69 h), the minimum distance is then 400 pc. This is more compatible with the low interstellar absorption derived from the X-rays.

The peculiar shape of the nIR spectrum is further confirmed by the surprising detection of IGR J1955 at IR wavelengths by the Wide-field Infrared Survey Explorer *WISE* (Wright et al. 2010) in all the four bands, W1 ($3.35\mu\text{m}$), W2 ($4.6\mu\text{m}$), W3 ($11.6\mu\text{m}$) and W4 ($22.1\mu\text{m}$) and catalogued as WISE J195512.47+004536.6. The corresponding magnitudes are $m_{W1} = 11.556 \pm 0.024$, $m_{W2} = 11.031 \pm 0.023$, $m_{W3} = 9.704 \pm 0.041$ and $m_{W4} = 8.506 \pm 0.31$. Most WDs detected by *WISE* (the *WISE* InfraRed Excesses around Degenerates, WIRED, survey project) are WD + Main Sequence binaries (Debes et al. 2011). Infrared excess around WDs could also be due to debris discs (Debes et al. 2012) or cyclotron emission in case of magnetic systems (Harrison et al. 2013). Therefore, we have combined the OM UV and B band photometry, the SDSS (u', g', r', i and z') and optical spectrum by Masetti et al. (2010) with the 2MASS (J, H and K) and *WISE* (W1, W2, W3 and W4) photometry to construct the spectral energy distribution (SED), although these measures are taken at different epochs.⁶ (see Fig.10). The SED is not corrected for extinction because, from the hydrogen column density of X-ray fits, it is at most $E_{(B-V)}=0.1$. Nevertheless, the unusual shape of the SED is apparent, with a pivot energy at $1.2\mu\text{m}$, where at shorter wavelengths the spectrum is a power-law $F_\nu \propto \nu^\alpha$, with $\alpha=0.9$ for the OM UV and B band data, and $\alpha=1.5$ for the SDSS data. The rapid rise of the flux beyond $1.2\mu\text{m}$ and the peak in the W1 ($3.35\mu\text{m}$) is very similar to that observed in the Polar EF Eri with *WISE* and *Spitzer* (Harrison et al. 2013). EF Eri is a short period (1.35 h) Polar believed to harbour a sub-stellar secondary star and which has been in a prolonged low state for a decade. The nIR and IR spectrum of EF Eri also does not give evidence of the secondary star but has been modeled as due to cyclotron emission from accretion onto a 12.6 MG WD (see Harrison et al. 2013, for more details). At these wavelengths the contribution comes from lower cyclotron harmonics ($n=1,2,3$), which are expected to be optically thick. The lack of nIR and IR spectroscopy does not allow a meaningful analysis of the spectrum of IGR J1955 with cyclotron models. Also, since EF Eri is strongly variable (more than a magnitude) in the nIR and IR along its orbital period, we have then inspected the "single exposure" observations from *WISE* survey. These were acquired along 1 d on Apr. 21, 2010. Useful data are reported for the W1, W2 and W3 bandpasses in Fig.11, that show large variations ($\Delta M > 1$ mag). Unfortunately the data are too sparse to phase them at either 1.38 h or 1.69 h periods.

Hence, the two short periodicities, the X-ray spectral characteristics and the striking similarity of the nIR and IR properties of IGR J1955 with EF Eri favours a magnetized CV accreting at a low accretion rate below the orbital period gap.

5 SUMMARY

We have presented the first long X-ray observations of the three new hard X-ray sources Swift J1907, IGR J1212 and IGR J1955 together with UV, optical, nIR and IR photometry.

⁶ The SDSS data were taken in Sept. 2004, the 2MASS data in Aug. 1999, the *WISE* photometry in Apr. 2010 and the optical spectroscopy in 2009.

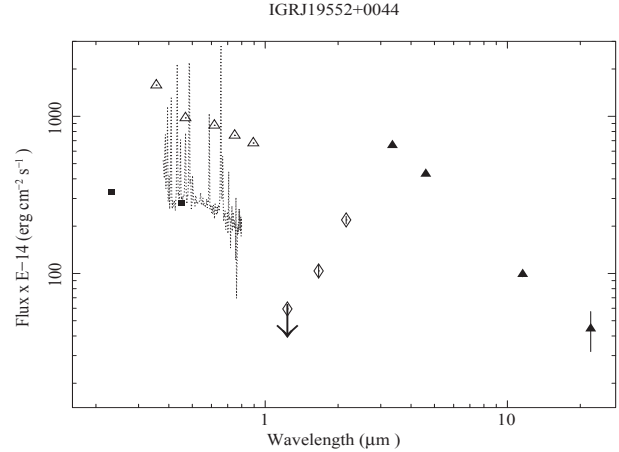


Figure 10. The SED of IGR J1955 constructed with the *XMM-Newton* UV and B band fluxes (filled squares), the optical spectrum by Masetti et al. (2010) (dotted line), the SDSS photometry (empty triangles), the 2MASS nIR (empty diamonds) and *WISE* measures (filled triangles). No correction for extinction is applied. The peculiar shape is discussed in the text.

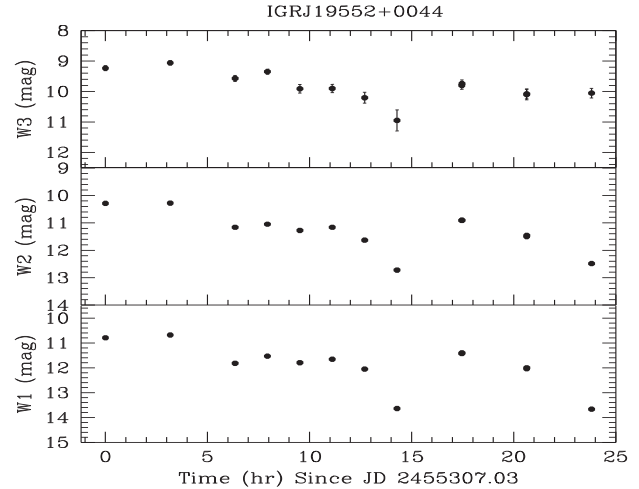


Figure 11. The *WISE* light curve of IGR J1955 constructed using the "single exposures" in the W1, W2 and W3 bandpasses, showing large IR variability

All three sources are hard X-ray emitting CVs that show large amplitude variabilities on timescales of minutes to hours. Two of them, Swift J1907 and IGR J1955, also show long (months to years) variabilities. Their broad-band X-ray spectra present characteristics typical of magnetic CVs. We here summarize the main results:

- Swift J1907 is a long (20.82 h) orbital period CV. We detected a non-coherent variability at a period of ~ 7200 s. It is likely of transient nature, reflecting matter traveling from the secondary star onto the compact object. Swift J1907 reveals a spectrum closely resembling those of magnetic CVs, including a soft X-ray component originating from a small fraction of the WD area. A magnetic system is then favoured although we cannot give a proper classification. The supra-solar abundance of nitrogen (about twice the solar value), the inverted mass ratio ($q=1.3$) and the long orbital period could suggest that Swift J1907 underwent a TTMT phase.
- IGR J1212 reveals a X-ray variability at $\gtrsim 7.6$ h that might reflect the binary orbital period. No fast coherent pulses are detected

though, but its spectral characteristics give support to a magnetic CV of the IP type.

- IGR J1955 shows two X-ray periods: 1.38 h and 1.69 h. Its X-ray spectrum indicates a system accreting at low rate similarly to the CVs below the orbital period gap. We have found IGR J1955 to display peculiar nIR and IR spectrum remarkably similar to that observed in the Polar EF Eri. We propose this system to be a pre-polar or an IP with the lowest degree of asynchronism, resembling the peculiar magnetic CV Paloma.

Our study of newly discovered CV candidates has revealed new features, departing from canonical view of magnetic CVs. In general, most of the hard X-ray discovered CVs are being found at relatively long orbital periods. This aspect deserves a detailed investigation to understand the evolutionary status of these CVs.

ACKNOWLEDGMENTS

This work is based on observations obtained with *XMM-Newton* an ESA science mission with instruments and contributions directly funded by ESA Member States; with *Swift*, a NASA science mission with Italian participation; and *Suzaku*, a collaborative mission between the space agencies of Japan (JAXA) and the USA (NASA). This publication also makes use of data products from the Wide-field Infrared Survey Explorer, which is a joint project of the University of California, Los Angeles, and the Jet Propulsion Laboratory/California Institute of Technology, funded by the National Aeronautics and Space Administration; the Two Micron All Sky Survey (2MASS), a joint project of the University of Massachusetts and the Infrared Processing and Analysis Center (IPAC)/Caltech, funded by NASA and the NSF; and the Sloan Digital Sky Survey (SDSS).

REFERENCES

Anzolin G., de Martino D., Bonnet-Bidaud J.-M., Mouchet M., Gänsicke B. T., Matt G., Mukai K., 2008, *A&A*, 489, 1243
 Anzolin G., de Martino D., Falanga M., Mukai K., Bonnet-Bidaud J.-M., Mouchet M., Terada Y., Ishida M., 2009, *A&A*, 501, 1047
 Barlow E. J., Knigge C., Bird A. J., J Dean A., Clark D. J., Hill A. B., Molina M., Sguera V., 2006, *MNRAS*, 372, 224
 Barthelmy S., 2000, in Flanagan K. A., Siegmund O., eds, Proc. SPIE Vol. 4140, X-ray and Gamma-Ray Instrumentation for Astronomy XI. p. 50
 Baumgartner W., Tueller J., Markwardt C., Skinner G., Barthelmy S., Mushotzky R., Evans P., Gehrels N., 2013, *ApJS*, 297, 19
 Bernardini F., de Martino D., Falanga M., Mukai K., Matt G., Bonnet-Bidaud J.-M., Masetti N., Mouchet M., 2012, *A&A*, 542, A22
 Beuermann K., Burwitz V., Reinsch K., 2012, *A&A*, 543, A41
 Beuermann K., El Kholly E., Reinsch K., 2008, *A&A*, 481, 771
 Bird A. J. et al., 2010, *ApJS*, 186, 1
 Cusumano G., La Parola V., Segreto A., Ferrigno C., Maselli A., Sbarufatti B., Romano P. e., 2010, *A&A*, 524, 64
 de Martino D. et al., 2013, *A&A*, 550, A89
 de Martino D. et al., 2010, *A&A*, 515, A25
 de Martino D. et al., 2008, *A&A*, 481, 149
 de Martino D., Matt G., Mukai K., Bonnet-Bidaud J.-M., Gänsicke B., Gonzalez-Perez J., Haberl F., Mouchet M. and Solheim J.-E., 2005, *A&A*, 437, 935

Debes J., Hoard D., Farihi J., S. W., Leisawitz D., Cohen M., 2012, *ApJ*, 759, 37
 Debes J., Hoard D., Wachter S., Leisawitz D., Cohen M., 2011, *ApJS*, 197, 38
 den Herder J. W. et al., 2001, *A&A*, 365, L7
 Dickey J. M., Lockman F. J., 1990, *ARA&A*, 28, 215
 Evans P. A., Beardmore A., Osborne J., O'Brian P., Willingale R. and Starling R., Burrows D. e. a., 2009, *MNRAS*, 397, 1177
 Ezuka H., Ishida M., 1999, *ApJS*, 120, 277
 Fischer A., Beuermann K., 2001, *A&A*, 373, 211
 Gänsicke B. et al., 2003, *ApJ*, 594, 443
 Gehrels N., Chincarini G., Giommi P., Mason K., Nousek J., Wells A., White N., Barthelmy S. e. a., 2004, *ApJ*, 611, 1005
 Harrison T., Hamilton R., Tappert C., Hoffman D., Campbell R., 2013, *AJ*, 145, 19
 Honeycutt R. K., Kafka S., 2004, *AJ*, 128, 1279
 Hong J., 2012, *MNRAS*, 427, 1633
 Hong J., van der Berg M., Grindlay J., Servillat M., Zhao P., 2012, *ApJ*, 746, 165
 Kalberla P. M. W., Burton W. B., Hartmann D., Arnal E. M., Bajaja E., Morras R., Pöppel W. G. L., 2005, *A&A*, 440, 775
 Koyama K. et al., 2007, *PASJ*, 59, 23
 Luna G. J. M., Sokolowski J. L., Mukai K., Nelson T., 2012, *ArXiv e-prints*
 Masetti N. et al., 2008, *A&A*, 482, 113
 Masetti N. et al., 2006, *A&A*, 459, 21
 Masetti N., Nucita A., Parisi P., 2012, *A&A*, 544, A114
 Masetti N. et al., 2012, *A&A*, 538, A123
 Masetti N. et al., 2010, *A&A*, 519, A96
 Mason K. O. et al., 2001, *A&A*, 365, L36
 McDermott P. N., Taam R. E., 1989, *ApJ*, 342, 1019
 Mitsuda K. et al., 2007, *PASJ*, 59, 1
 Morihana J., Tsujimoto M., Yoshida T., Ebisawa K., 2013, *ApJ*, 766, 14
 Nauenberg M., 1972, *ApJ*, 175, 417
 Nebot Gómez-Morán A. et al., 2013, *A&A*, 553, A12
 Norton A. J., Butters O., Parker T., Wynn G. A., 2008, *ApJ*, 672, 524
 Norton A. J., Wynn G. A., Somerscales R. V., 2004, *ApJ*, 614, 349
 Peterson B., Wanders I., Horne K., Collier S., Alexander T., Kaspi S., Maoz D., 1998, *PASP*, 110, 660
 Podsiadlowski P., Han Z., Rappaport S., 2003, *MNRAS*, 340, 1214
 Pretorius M. L., Knigge C., Schwöpe A. D., 2013, *MNRAS*, 432, 570
 Ramsay G., Wheatley P. J., Norton A. J., Hakala P., Baskill D., 2008, *MNRAS*, 387, 1157
 Reis R., Wheatley P., Gänsicke B., Osborne J., 2013, *MNRAS*, 430, 1994
 Revnitvsev M., Sazonov S., Forman W., Churazov E., Sunyaev R., 2011, *MNRAS*, 414, 495
 Ryter C., Cesarsky C. J., Audouze J., 1975, *ApJ*, 198, 103
 Scargle J. D., 1982, *ApJ*, 263, 835
 Scaringi S., Connolly S. Patterson J., Thorstensen J., Uthas H., Knigge C., Vican L., Monard B., Rea R. e., 2011, *A&A*, 530, A6
 Schenker K., Wynn G. A., Speith R., 2004, in Vriellmann S., Cropper M., eds, ASP Conf. Ser. Vol. 315, IAU Colloq. 190: Magnetic Cataclysmic Variables. p. 8
 Schwarz R., Schwöpe A., Staude A., Rau A., Hasinger G., Urrutia T., Motch C., 2007, *A&A*, 473, 511
 Shang Y., 2002, *MNRAS*, 337, 609
 Smith D., Dhillon 1998, *MNRAS*, 301, 767

- Straizys V., Lazauskaitė R., 2009, *Baltic Astronomy*, 18, 19
Suleimanov V., Revnivtsev M., Ritter H., 2005, *A&A*, 435, 191
Thorstensen J. R., Peters C. S., Skinner J. N., 2010, *PASP*, 122, 1285
Turner M. J. L. et al., 2001, *A&A*, 365, L27
van Paradijs J., Verbunt F., 1984, in Woosley S. E., ed., *AIP Conf. Ser. Vol. 115, High Energy transients in Astrophysics*. p. 49
Warner B., 1995, *Cambridge Astrophysics Series*, 28
Wickramasinghe D. T., Ferrario L., 2000, *PASP*, 112, 873
Woelk U., Beuermann K., 1996, *A&A*, 306, 232
Wright E. L. et al., 2010, *AJ*, 140, 1868
Zorotovic M., Schreiber M., Gänsicke B., 2011, *A&A*, 536, A42